applied sciences

MDPI

Article

Driven Pile Effects on Nearby Cylindrical and Semi-Tapered Pile in Sandy Clay

Massamba Fall, Zhengguo Gao * and Becaye Cissokho Ndiaye

School of Transportation Science and Engineering, Beihang University, Beijing 100083, China; lb1613205@buaa.edu.cn (M.F.); ndiayebecaye@buaa.edu.cn (B.C.N.)
* Correspondence: gaozg@buaa.edu.cn

Abstract: A pile foundation is commonly adopted for transferring superstructure loads into the ground in weaker soil. They diminish the settlement of the infrastructure and augment the soil-bearing capacity. This paper emphases the pile-driving effect on an existing adjacent cylindrical and semi-tapered pile. Driving a three-dimensional pile into the ground is fruitfully accomplished by combining the arbitrary Lagrangian–Eulerian (ALE) adaptive mesh and element deletion methods without adopting any assumptions that would simplify the simulation. Axial forces, bending moment, and lateral displacement were studied in the neighboring already-installed pile. An investigation was made into some factors affecting the forces and bending moment, such as pile spacing and the shape of the already-installed pile (cylindrical, tapered, or semi-tapered). An important response was observed in the impact of the driven pile on the nearby existing one, the bending moment and axial forces were not negligible, and when the pile was loaded, it was recommended to consider the coupling effect. Moreover, the adjacent semi-tapered pile was subjected to less axial and lateral movement than the cylindrical one with the same length and volume for taper angles smaller than 1.0°, and vice versa for taper angles greater than 1.4°.

Keywords: pile driving; semi-tapered pile; cylindrical pile; axial response; bending moment

Citation: Fall, M.; Gao, Z.; Ndiaye, B.C. Driven Pile Effects on Nearby Cylindrical and Semi-Tapered Pile in Sandy Clay. *Appl. Sci.* **2021**, *11*, 2919. https://doi.org/10.3390/app11072919

Academic Editor: Chiara Bedon

Received: 11 February 2021
Accepted: 20 March 2021
Published: 25 March 2021

1. Introduction

Piles could be adopted as a deep foundation for transferring loads of structures into the ground. They are commonly used when the ground is not able to support the structures individually. During earthquakes, some structures supported by a pile foundation collapse sometimes [1]. These collapses could be related to the exclusion of axial forces from some codes. Different techniques could be adopted for pile installations inside the ground going from drilling holes, boring, jacking, and driving the pile or cast in place. The driven pile is broadly adopted in modern engineering practices (improves the soil in case of seismic hazards and increases the soil stiffness in the weaker zone) and gained popularity in the past years because of their large tip and skin resistance [2,3]. Sadly, driven piles are associated with vibrations during the installation, noise, and reduced resistance issues [4]. Poulos [5] revealed that the driving of a pile involves a ground movement which will result in additional forces, bending moment, and displacement of nearby foundation structures. Severe damage or collapse of structures have been noticed after earthquakes, especially in weaker soil areas [1,6]. The bending moment and axial force experienced by piles during the event would have exceeded the bending moment and axial force of the section.

Tapered or semi-tapered piles are characterized by a difference at the bottom and top of the axial pile diameter. They are adopted into real engineering given the limited ground vibrations during the driving process. Tavasoli and Ghazavi, and Sormeie and Ghazavi [7,8] studied the ground motion related to tapered, cylindrical, and semi-tapered piles driven into the ground. The results showed that the non-uniform pile cross-section reduced working time, noise, and energy consumption. Nonetheless, the performance of tapered piles subjected to loading is not fully understood. Under harmonic loading,

lateral loading, and earthquake loading, the use of cylindrical piles displayed a worse performance than the tapered piles with the same length and volume [9–12]. None of these previous researchers have studied the performance of tapered piles during the driving of nearby pile foundations.

Driven piles have been studied by adopting laboratory tests [13,14] and numerical simulations [15–17]. A laboratory test does not give the deformations and stresses in the whole model. It can just be a tool to reasonably predict ground movement. The numerical simulation could be applied to get a large view of the ground, structure deformations, and movement. Nevertheless, its application during nonlinear plasticity soil behavior (for example, driven piles inside the ground) is complicated. In light of this, some simplified assumptions are generally adopted in regard to pile driving. In [18–20], the pile was simulated as a rigid body to ease the driving process. According to this hypothesis, the Young's modulus value of the pile is large compared to the soil one. This large stiffness of the pile allows its easy penetration inside the soil. To limit the soil distortion during the pile penetration, Dijkstra et al. [21] proposed an approach to make the soil flow around the pile while the pile is being fixed. Unrealistic boundary conditions were assumed by this technic. Another approach is to model a small radius tube in the pile centerline [22]. A pre-bored hole with varying depth could be adopted to complete the driving process [23–28]. Hence, discontinuous pile driving was realized instead of a continuous one. All these simplified assumptions assumed a nonrealistic model of the pile–soil interaction and might deviate the results from the field monitoring values. Their elimination could lead to better results compared to the field test.

Braced excavation, deep excavation, and tunneling effects on adjacent pile foundations were studied by [29–37]. These constructions may adversely affect nearby piles. The lateral loads, resulting in soil movement, induce axial forces, deflection, bending moment, settlement, and lift-off of the surrounding pile foundation, which may lead to structural failure, crack, and distress. Axial forces and lateral effects could be adopted to observe the corresponding pile deformation [30]. Goh et al. and Liyanapathirana and Ravin [29,32] studied the pile damage induce by deep excavation adopting the bending moment and the pile deflection. Charles et al. [31] showed that the settlement and shaft resistance deserves more investigation. Bending moment, axial force, settlement, and lateral movement were observed by Soomro et al. [34] to study the pile behavior during adjacent excavation. The parameters deserve more investigation into nearby located piles. Hence the construction of new structures has not been fully understood. However, all these researchers adopted a static analysis by neglecting the dynamic effect, which was induced by engines and working conditions.

In this study, a three-dimensional driven pile is looked at by adopting the arbitrary Lagrangian–Eulerian (ALE) adaptive mesh and element deletion methods available in Abaqus [38]. Any assumptions that simplify the simulation were drawn, resulting in a reliable way to simulate the soil–pile interaction. The obtained results were close to the field measurements. Furthermore, the axial force, bending moment, and lateral movement of a nearby already-installed pile were observed during the driving process. An examination of some factors impacting the forces and bending moment, such as pile shape (cylindrical or semi-tapered pile) and pile spacing was conducted. It was concluded that parameters deserve more investigation during pile driving in regard to the adjacent existing pile.

2. Basic Concepts

2.1. Factors for Ground Vibration Estimation

Peak particle acceleration (PPA), displacement (PPD), and velocity (PPV) could be used to estimate the ground vibrations. PPV can better evaluate the structure's start of damage than PPD and PPA. It is generally used for measuring structure damage [39,40]. Regarding the evaluation in terms of velocity, the maximum is one experience by particle subjected to vibration. PPV can be evaluated by:

Peak vertical velocity [41–44]:

$$PPV = V_{V\max} \quad (1)$$

2.2. Wave Propagation and Determination of Soil Damping Ratio

Damping is a vast topic in dynamics; it tends to be confused with phenomena that produce amplitude reduction. In a static analysis, the deflection of the structure is controlled by stiffness. Nevertheless, in dynamic analysis, the response switches between damping, mass, or stiffness. Damping is essential for calculating the response of the structures subjected to dynamic excitation [45]. Madheswaran et al. [46] revealed that the extreme of the vibration energy affecting adjacent structures was transferred by the Rayleigh waves that circulate near the ground surface. The waves generated by vibrations reproduce in the soil and could interrelate and damage adjacent constructions. It also could induce liquefaction, densification, and permanent settlement in the soil. The circulating waves close to the pile could be divided into (1) on the surface: the Rayleigh wave; (2) around the pile toe: the body wave; and (3) around the shaft: the vertical shear wave. Far away from the field, the soil response was controlled by the Rayleigh waves, and the body waves were considerably reduced. Near the field, the response of the soil was controlled by the shear waves [47].

2.3. Soil–Pile Interaction

The friction coefficient of the pile is evaluated according to the type of pile (steel or concrete), the type of soil (fine or coarse), and their properties. For sandy clay and concrete piles, the value varies between 0.2 and 0.4. They were conferring to the Technical Manual TM 3–34.22 (U.S. Army 2013). Farshi and Hamidi [16] proved that an augmentation in PPV conducted an upsurge friction coefficient principally near to the pile axis. Therefore, the friction coefficient reduction by adopting a steel pile rather than a concrete pile induced attenuation of ground vibrations. The pile–soil friction coefficient was taken as 0.35 in this paper, according to [15,16,48].

2.4. Evaluation of Pile Axial Ultimate Capacity

Methods for evaluating the pile's ultimate capacity in compression generally involve adding the end-bearing capacity to the shaft resistance (McCarron [49]).

$$Q_t = \pi D \int_{Z=0}^{Z=L} f(z)dz + \pi D^2 q/4 \quad (2)$$

where D = diameter of the pile, q = unit end bearing, and $f(z)$ = unit skin friction.

However, in this study, the piles were installed through the driven process; only the skin friction was mobilized (the shaft resistance was exclusively evaluated in this work). The final pile installation depth did not reach the bedrock. Equation (2) is simplified as

$$Q_t = \pi D \int_{Z=0}^{Z=L} f(z)dz \quad (3)$$

The unit skin friction can be evaluated using Equation (4). $f(z) = \delta S_u$ (4) where α is a coefficient without dimension and S_u is evaluated at the point in question and nominated the undrained shear strength of the soil. The formula proposed by the American Petroleum Institute API (1984, 1987) advocates values for δ in relation to c_u as follows

$$\delta = \begin{cases} 1 - \frac{c_u - 25}{90} & for\ 25\ \text{kPa} \le c_u \le 70\ \text{kPa} \\ 1 & for\ c_u \le 25\ \text{kPa} \\ 0 & for\ 70\ \text{kPa} \le c_u \end{cases} \quad (4)$$

Using the Mohr–Coulomb failure criterion the undrained shear strength is:

$$s_u = c + \sigma \tan(\phi) \quad (5)$$

$$\text{And } \sigma = \frac{\sigma_1 + \sigma_3}{2} \quad (6)$$

where $\sigma_1 = k\gamma z$ and $\sigma_3 = \gamma z$. k is the lateral earth pressure factor, γ is the soil density, and z is the depth of the point in question. k can be evaluated by [34,50] $k = 1 - \sin(\phi)$ $Q_t = 802.34$ kN.

3. Numerical Model and Verification

The analysis method used in this paper involved two steps: (1) driving a single pile into the soil without any other structures and comparing the results with the field measurement presented by Wiss (1981) [51]; (2) driving the pile adjacent to the nearby existing pile and carrying out parametric studies on the pile shape and pile spacing effects, pile bending moment, axial force, and lateral movement. The Abaqus/explicit [38] was adopted to drive the pile from the initial depth to the final position. A three-dimensional model was chosen to complete the simulation phase, and the results were compared with the case study by Wiss (1981).

The driven pile induced soil movement, which developed a bending moment and axial forces on the existing nearby piles. Damage or cracking (concrete pile) could occur caused by these developed forces. The response of the adjacent piles during the vibration procedures could be studied by means of parametric values such as pile shape and pile spacing to observe the influence of these parameters on the generated axial forces, bending moment, and lateral movement. Commonly, the pile is driven until it reaches a harder stratum. Figure 1 shows the fundamental problem and describes some of the same parameters of the geometric as the one provided by [51].

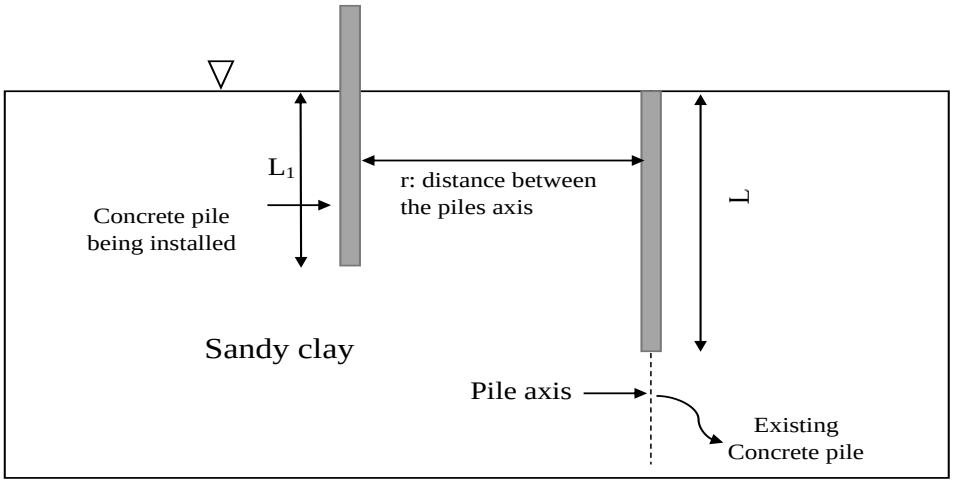

Figure 1. Driven pile near the already-installed pile.

Figures 2 and 3 show the geometry of the soil and pile models. A uniform soil layer was taken (sandy clay), the diameter of the concrete pile was 0.5 m, the length was evaluated as 10 m, and 60° was taken as the conical tip angle. A total of 25,120 nodes and 25,120 elements were used to build the model.

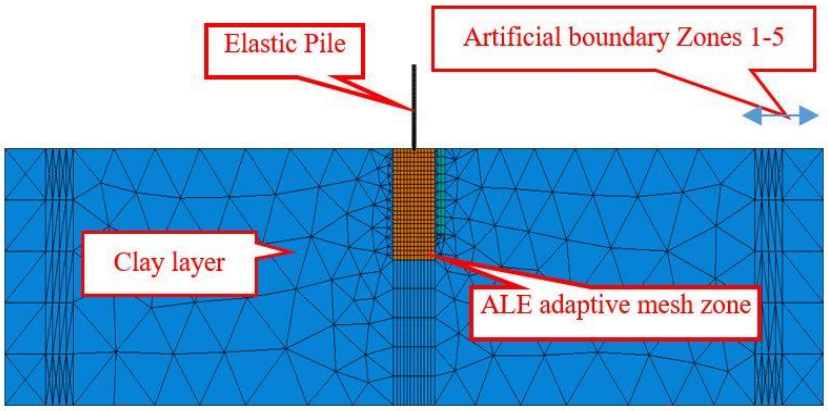

Figure 2. Two-dimensional section of the model.

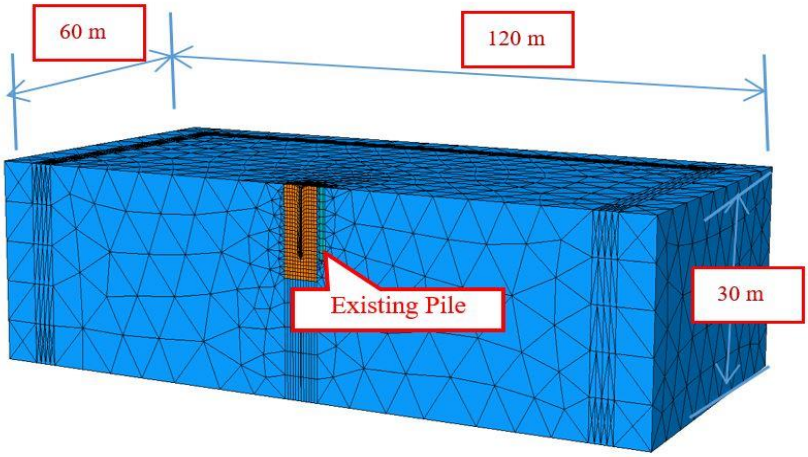

Figure 3. Three-dimensional model equivalent.

The material properties adopted are listed in Table 1. Their characteristics were the same as the model proposed by [15,51,52]. Hence, the reliability of the method was evaluated by comparing the results with the field measurement presented by Wiss (1981). An elastic model was used to capture the pile behavior, and the Drucker–Prager model was used to define the elastoplastic behavior of the soil with the friction angle (ϕ) set to 25°, the flow stress ratio (K) set to one, and the dilation angle (ψ) set to 1°. Due to the computer size limitation during the dynamic simulation, only one part of the model was mapped in a computational domain. Generally, the part of the ground that was expected to have a significant effect was mapped. The remaining area was taken into account in the definition of the boundary conditions, which intended to limit the wave reflection. These boundary conditions were intended to capture the wave reflection during a dynamic simulation of pile driving. The reflection of the outward-propagating wave could be caused by the fixed boundary conditions, by adding energy inside the model.

Table 1. Soil and pile material properties.

Elastic Pile				
Diameter	Length	Density	Young's modulus	Poisson's ratio
0.5 m	10 m	2500 kg/m^3	40,000 MPa	0.25
Sandy Clay				
Friction angle	Cohesion	Density	Young's modulus	Poisson's ratio
25 degrees	15 kPa	2000 kg/m3	80 MPa	0.4

An infinite element at the side and bottom part of the finite element mesh to prevent wave reflection was used in [17,20]. The boundary element was proposed by [47] to capture the soil behavior. Other papers used artificial boundaries to absorb the wave deriving from the driven pile [15,16,48,52]. A regular augmentation of the damping was adopted for absorbing the wave and its limited the errors before model verification [53]. An artificial boundary can be summarized in the following steps:

1. Divide the side and bottom part of the finite element mesh into subzones
2. Increase the damping gradually in these subzones

Figure 2 shows the five subzones of the artificial boundary definition to avoid a reflection of the wave.

The damping was gradually increased in these zones from 7.5–17.5%. Zhang and Tao evaluated the limit of the Rayleigh damping from 2.4–15.4% for clays and from 1.5–17.5% for sands. The soil damping was taken as 7% as provided by [15,16] for a similar soil layer. The depth of the soil was seized large enough to allow the natural damping of the waves at the bottom boundary.

Driving a pile is a process that involves large deformation in the soil surrounding the pile toe. This caused soil distortion and resulted in the abortion of the simulation. Therefore, an ALE technic was used to prevent abortion of the calculation. The use of the ALE could change the system over time (Figure 2). The element mesh shape is optimized due to its erratic movement. Both the arbitrary Lagrangian–Eulerian zone and pile were modeled using C3D8R (8-node linear brick elements with reduced integration and hourglass control coefficients reduction), and the rest of the soil layer was modeled using tetrahedral mesh. Furthermore, due to the large displacement in the soil zone surrounding the pile toe, an ALE mesh was carried-out to permit an automatic re-mesh for optimizing the element shape and to avoid cessation of the simulation afterward due to large element distortion. The element deletion technic was also adopted to delete the element that failed.

Modeling the hammer impact directly beyond some simplifications could be fastidious due to the complex equipment of the impact hammer (ram, cushion, and an anvil). Some analytical method representing each impact hammer was developed to simplify the simulation formula. The model given by Deeks and Randolph (1993) [54] was used to find the equivalent concentrated force for each hammer at the pile head blow (Figure 4).

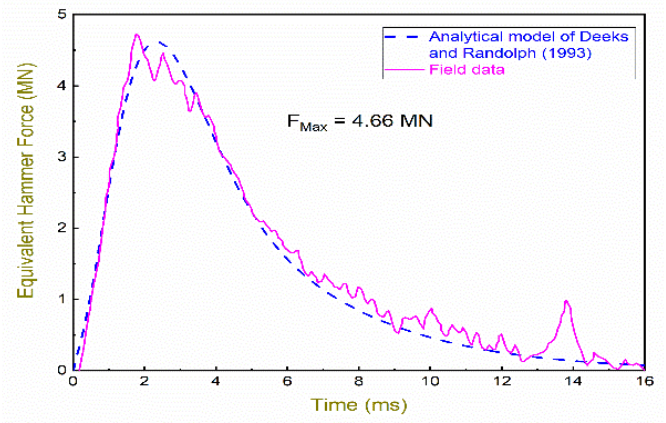

Figure 4. Impact force hammer BSP 357 versus time.

The driven-pile installation from the initial position to the final depth was realized in three steps: (1) running the initial conditions of the site by applying gravity load, (2) taking a short time of 0.25 s to permit a primary pile penetration inside the soil caused by its weight, and (3) executing successive impact hammering on the head of the pile until it reached its final penetration depth.

The validity of the numerical simulation should be estimated by comparing some results with previous evaluated field monitoring results. The closeness of the results to the

field measurement was the criteria that defined the reliability of the results. The recorded values by Wiss (1981) were adopted to approve the proposed method. The comparison between the peak particle velocity (PPV) of numerical and measure values was conducted at some radial distances from the surface of the ground, as plotted in Figure 5. Conferring to Figure 5, the simulation results were feasible using the field measurement. The simulated and experienced PPV values were compared in a large distance of 1–45 m, to assure the reliability of the results.

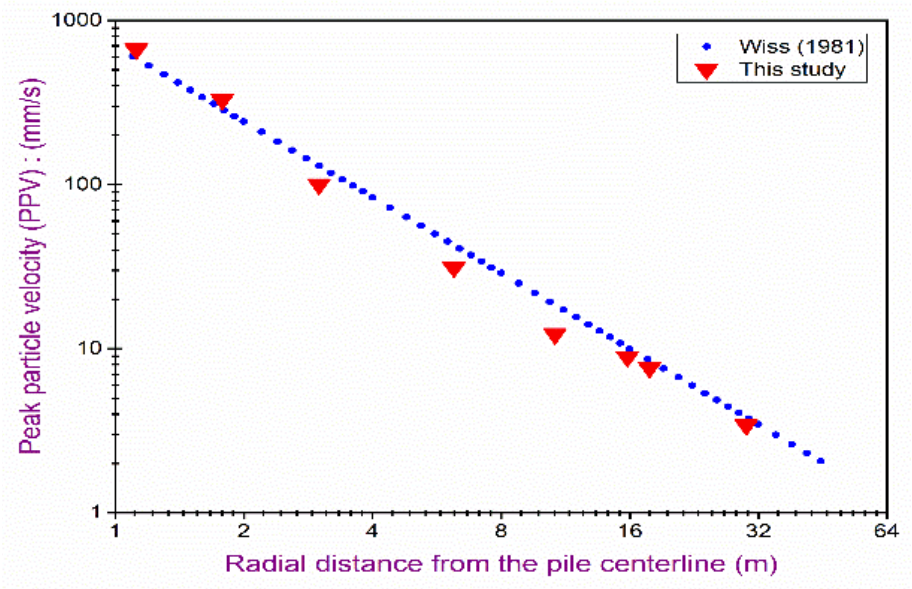

Figure 5. Peak particle velocity (PPV) measurements presented by Wiss [51] and computations caused by driving the pile into soil particles located at the ground surface.

4. Pile Response Analysis Due to Ground

4.1. Axial Reaction

The pile was modeled as a three-dimensional finite element. A 4-node doubly curved thick or thin shell, finite membrane strains, hourglass control, and reduced integration (S4R) were adopted to model the pile. The sandy clay soil parameters were considered reasonably typical for medium-stiff clay. Some simplifications were applied in many approaches, in particular: (1) Young's modulus was taken for the pile-skin friction and soil constant with depth; (2) the effects of the driven pile were manifested in horizontal displacements at the existing pile location, and as statically vertical. No attention was set to the potential dynamic impacts emanating while driving the pile. The moment and axial forces were the integration of the shell stresses, and they were given per unit length for the element.

At the beginning of the simulation, the soil moved downwards (taken negative in this paper); nonetheless, when the penetration upsurged, the soil adjacent to the surface moved positively, and a heave happened. At the end of the simulation ($L_1/L = 1$), a heave arose in the soil at all levels. In analyzing these responses, a sequential (subsequent) additional calculation was completed beginning from a primarily stress-free pile, and pertaining the free-field movements in order for three pile penetration depths $L_1/L = 1/3$, $2/3$, and 1. Thus, the preceding soil movement effect could be appropriately taken into account.

For one case ($r/d = 8$, d is the diameter of the pile), Figure 6 displays the simulated behaviors of the existing friction pile axial force. The pile's axial force increased with the driven pile penetration inside the soil, and (L_1) upsurged until the ratio ($L_1/L = 0.7$) when the axial force diminished with the length of penetration increased. The maximum compressive force was about 56.2% of the ultimate geotechnical shaft resistance of approximately 802.3 kN.

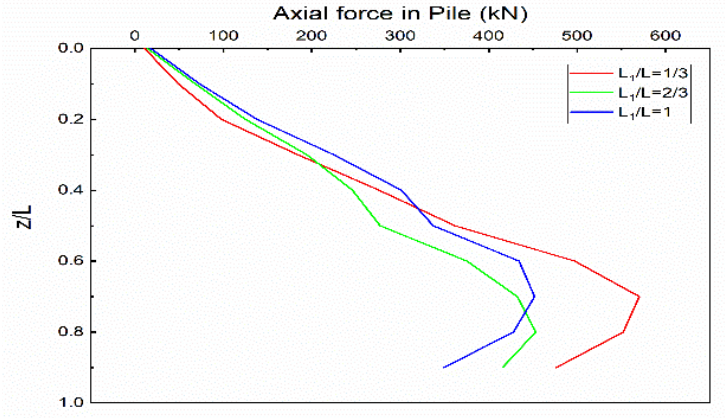

Figure 6. Axial force distribution in the friction pile caused by the driving of a nearby pile.

4.2. Bending Moment Analysis

Figure 7 plots the simulated behavior of the produced bending moment in the existing pile for penetration depths L_1/L of the newly installed pile. The already-installed pile's head and tip were free for movement. The bending moment values were significant when positioning the pile at r/d = 8 (nearby the driven pile), particularly for relatively large values of L_1/L. The maximum value increased and fluctuated while the driven pile attended its final depth of penetration. Hence, when the head and tip of the existing pile were free to move, the analyses clearly showed the possibility of damage to the already-installed pile while a pile was driven adjacently. In addition, the pile was modeled to behave elastically, thus the simulated bending moments could surpass the values that would induce the yielding of the pile.

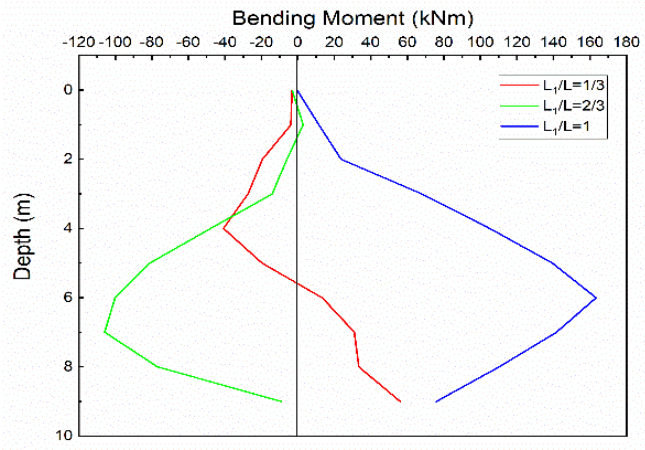

Figure 7. Bending moment simulation of distributions of in existing free-head pile caused by driving of a pile nearby.

4.3. Lateral Movement Analysis

The already-installed pile head and tip were free to move. Figure 8 displayed the simulated behavior of the produced lateral movement in a pile for three penetration depths L_1/L of the newly driven pile. A significant displacement value was noticed in a pile when positioning at r/d = 8, particularly at the end of the driving process ($L_1/L = 1$). The maximum value increased while the driven pile attended its final depth of penetration. At the pile depth of penetration, the maximum lateral displacement inside the existing pile was located approximated at the pile depth equal to the depth of penetration of the driven pile (Figure 8). This result is similar to the model proposed by Ni et al. [55].

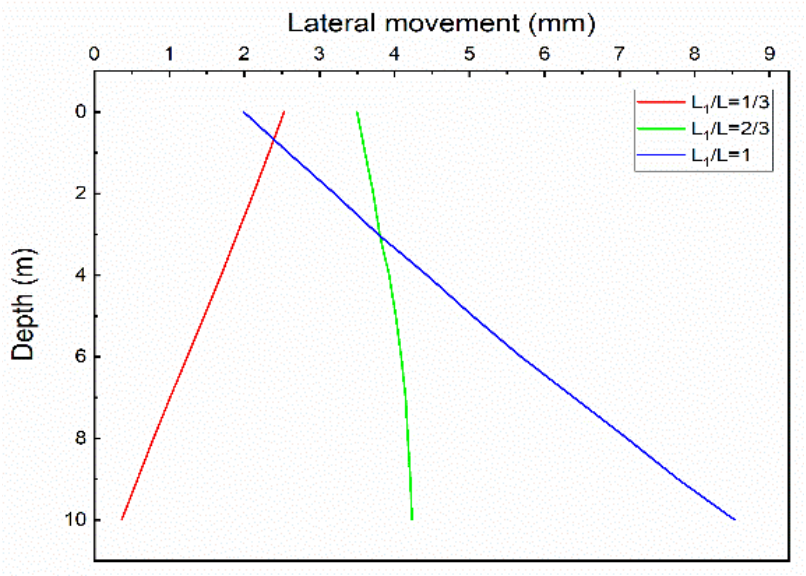

Figure 8. Simulated distribution of vertical soil movement adjacent to friction pile.

For small penetrations, the pile moved downward; however, for large penetrations L_1/L of the driven pile bigger than around 0.5, the already existing pile movement was upward. When (L_1/L = 1), a maximum value of the upward movements was attended (around 3% of the pile diameter) at a position of r/d = 8. Therefore, a fairly possible problem was observed when constructing the friction pile: (1) a heave would occur next to the existing pile, and (2) it could induce a loss of contact among the supporting soil and the pile tip and could induce the apparition of a gap. Once the load was applied on the pile and the resistance of the shaft was assembled entirely, a noticeable settlement could appear when the gap was closed previous to the tip re-touching the soil. These phenomena had been well-recognized and experienced in real engineering. The maximum lateral displacement decreased rapidly with an increase in r/d and became relatively small for spacings over around eight diameters. As plotted in Figure 9, the maximum displacement occurred for depths of penetration (L_1/L) of about one.

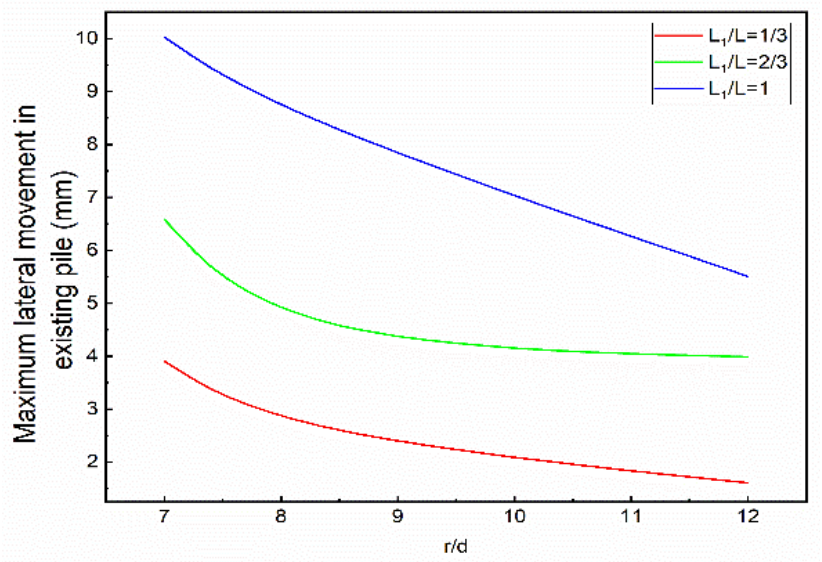

Figure 9. The impact of pile positioning on the maximum lateral displacement caused by a nearby driven pile.

4.4. Effect of the Pile Shape

Data about tapered and semi-tapered pile behavior during adjacent pile construction are scarce. In this section, the bending moment, axial force, and lateral movement on non-uniform pile cross-sections were caused by the driving of a friction pile. However, cylindrical and semi-tapered concrete piles with different geometries in terms of volume and length were adopted, as plotted in Figure 10. The cylindrical pile was 10 m long and 0.5 m thick. The semi-tapered pile was identical in volume and length to the cylindrical one and with the taper angle α taken as 0.7°, 1.0°, and 1.4° as proposed by Manandhar and Yasufuku [56]. Thus, the obtained results may be used in practice.

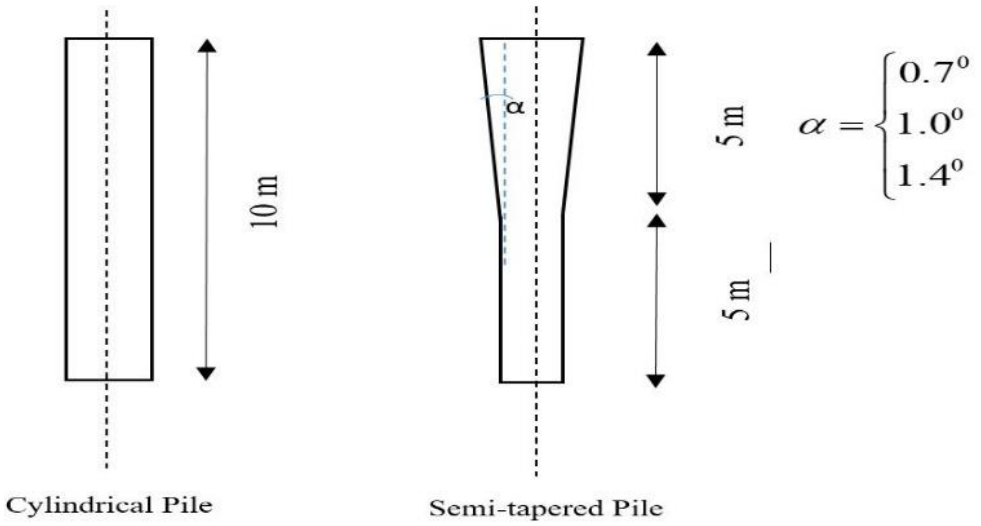

Figure 10. The geometry of concrete piles.

From the obtained results, it was concluded that the semi-tapered pile was subjected to less axial forces and lateral movement than the cylindrical one with the same length and volume for a taper angle of less than 1.0° (Figures 11 and 12). For the taper angle with more than 1.4°, large values of axial force and lateral movement were observed in the semi-tapered pile. Thus, the use of semi-tapered piles will be more beneficial than the cylindrical one with the same volume and length for a taper angle of less than 1.0°.

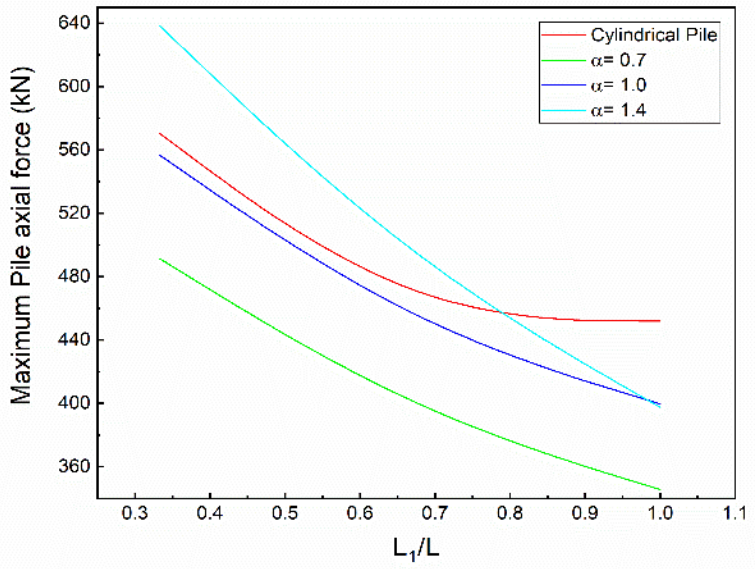

Figure 11. Maximum axial force for different pile shapes.

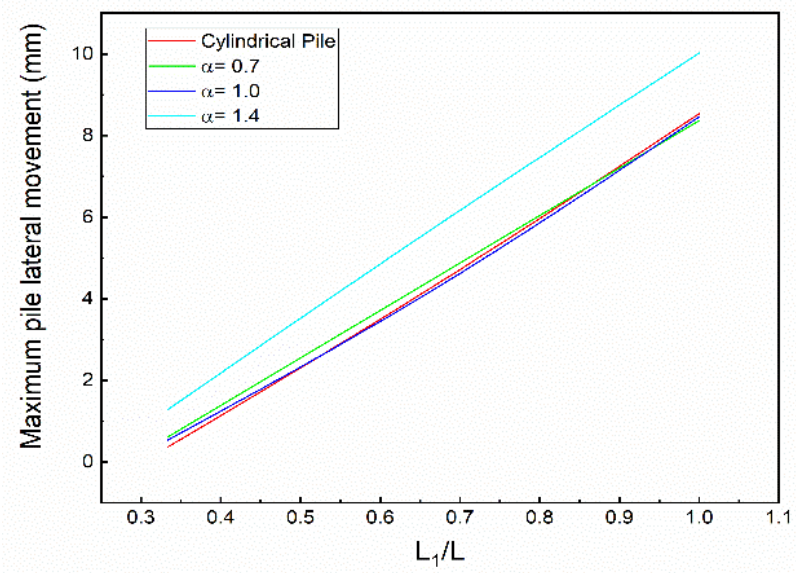

Figure 12. Maximum lateral movement for different pile shapes.

5. Conclusions

The study provided that the soil movements due to a driven pile can induce a large bending moment, lateral movement, and axial forces in an existing adjacent pile. Numerical simulation was adopted to evaluate these movements and forces.

1. In this paper, a reliable method to complete the driving of a pile was proposed. This involved combining the element deletion and arbitrary Lagrangian–Eulerian (ALE) mesh method.
2. The adjacent semi-tapered pile was subjected to less axial and lateral movement than the cylindrical one with the same length and volume for a taper angle smaller than 1.0°, and vice versa for a taper angle greater than 1.4°.
3. Moreover, the influence of the driven pile on the existing pile's responses was significant, the bending moment and axial force were not negligible, and the coupling effect in the case of the loaded pile should be factually considered. In fact, the pile's design subjected to lateral and axial load was usually treated as a separate problem.

Author Contributions: Conceptualization, Z.G. and M.F.; methodology, M.F.; software, M.F. and B.C.N.; validation, Z.G., M.F., and B.C.N.; formal analysis, M.F.; M.F., and B.C.N.; writing—original draft preparation, M.F.; writing—review and editing, Z.G. and B.C.N.; supervision, Z.G.; funding acquisition, Z.G. All authors have read and agreed to the published version of the manuscript.

Funding: This work was supported by the National Natural Science Foundation of China (11472029), (11872092), and the Beihang University.

Institutional Review Board Statement: Not applicable.

Informed Consent Statement: Not applicable.

Data Availability Statement: All the used data were available in the literature.

Conflicts of Interest: The authors declare no conflict of interest.

References

1. Bhattacharya, S.; Dash, S.; Mitra, N.; Adhikari, S.; Blakeborough, A. Investigation of Bending–Buckling Interaction of Piles in Liquefiable Soils. In Proceedings of the 14th World Conference on Earthquake Engineering, Beijing, China, 12–17 October 2008.
2. Meyerhof, G.G. Closure to "Bearing Capacity and Settlement of Pile Foundations". *J. Geotech. Eng. Div.* **1977**, *103*, 1023–1025. [CrossRef]
3. O'Neill, M.W. Review of augered pile practice outside the United States. In *Transportation Research Record1447*; Transportation Research Board: Washington, DC, USA, 1994; pp. 3–9.

4. Thiyyakkandi, S.; McVay, M.; Bloomquist, D.; Lai, P. Measured and Predicted Response of a New Jetted and Grouted Precast Pile with Membranes in Cohesionless Soils. *J. Geotech. Geo Environ. Eng.* **2013**, *139*, 1334–1345. [CrossRef]
5. Poulos, H. The influence of construction "side effects" on existing pile foundations. *Geotech. Eng.* **2005**, *36*, 51–67.
6. Lombardi, D.; Dash, S.; Bhattacharya, S. Inclusion of axial load on bending response of pile in liquefiable soils. In Proceedings of the 8th International Conference on Urban Earthquake Engineering, Tokyo, Japan, 7–8 March 2011.
7. Tavasoli, O.; Ghazavi, M. Wave propagation and ground vibrations due to non-uniform cross-sections piles driving. *Comput. Geotech.* **2018**, *104*, 13–21. [CrossRef]
8. Sormeie, A.; Ghazavi, M. Analysis of non-uniform piles driven into cohesive soils. *Soil Dyn. Earthq. Eng.* **2018**, *109*, 282–285. [CrossRef]
9. Ghazavi, M. Response of tapered piles to axial harmonic loading. *Can. Geotech. J.* **2008**, *45*, 1622–1628. [CrossRef]
10. El Naggar, M.H.; Wei, J.Q. Response of tapered piles subjected to lateral loading. *Can. Geotech. J.* **1999**, *36*, 52–71. [CrossRef]
11. Ghazavi, M. Analysis of kinematic seismic response of tapered piles. *Geotech. Geol. Eng.* **2006**, *25*, 37–44. [CrossRef]
12. Shanker, K.; Basudhar, P.; Patra, N. Flexural Response of Tapered Piles in Liquefied Soils. In Proceedings of the 12th International Conference of International Association for Computer Methods and Advances in Geomechanics, Goa, India, 1–6 October 2008.
13. Musir, A.A. A study of pile driving effects on nearby building. *Int. J. Geomate* **2014**, *6*, 806–810. [CrossRef]
14. Yang, Z.X.; Jardine, R.J.; Zhu, B.T.; Rimoy, S. Stresses Developed around Displacement Piles Penetration in Sand. *J. Geotech. Geo Environ. Eng.* **2014**, *140*, 04013027. [CrossRef]
15. Rooz, A.F.H.; Hamidi, A. A numerical model for continuous impact pile driving using ALE adaptive mesh method. *Soil Dyn. Earthq. Eng.* **2019**, *118*, 134–143. [CrossRef]
16. Rooz, A.F.H.; Hamidi, A. Numerical Analysis of Factors Affecting Ground Vibrations due to Continuous Impact Pile Driving. *Int. J. Géoméch.* **2017**, *17*, 04017107. [CrossRef]
17. Rezaei, M.; Hamidi, A.; Rooz, F.H.A. Investigation of Peak Particle Velocity Variations during Impact Pile Driving Process. *Civ. Eng. Infrastruct. J.* **2016**, *49*, 59–69. [CrossRef]
18. Sheng, D.; Eigenbrod, K.D.; Wriggers, P. Finite element analysis of pile installation using large-slip frictional contact. *Comput. Geotech.* **2005**, *32*, 17–26. [CrossRef]
19. Masoumi, H.R.; François, S.; Degrande, G. A non-linear coupled finite element-boundary element model for the prediction of vibrations due to vibratory and impact pile driving. *Int. J. Numer. Anal. Methods Géoméch.* **2009**, *33*, 245–274. [CrossRef]
20. Khoubani, A.; Ahmadi, M.M. Numerical study of ground vibration due to impact pile driving. *Proc. Inst. Civ. Eng. Geotech. Eng.* **2014**, *167*, 28–39. [CrossRef]
21. Dijkstra, J.; Broere, W.; Heeres, O. Numerical simulation of pile installation. *Comput. Geotech.* **2011**, *38*, 612–622. [CrossRef]
22. Grabe, J.; Henke, S. Simulation of pile driving by 3-dimensional Finite-Element analysis. In Proceedings of the 17th European Young Geotechnical Engineers' Conference, Croatia, Zagreb, 19–23 July 2006; pp. 215–233.
23. Mabsout, M.E.; Tassoulas, J.L. A finite element model for the simulation of pile driving. *Int. J. Numer. Methods Eng.* **1994**, *37*, 257–278. [CrossRef]
24. Ramshaw, C.L.; Selby, A.R.; Bettess, P. Ground Waves Generated by Pile Driving, and Structural Interaction. In Proceedings of the Fourth International Conference on Recent Advances in Geotechnical Earthquake Engineering and Soil Dynamic, St. Louis, MO, USA, 26–31 March 2001.
25. Masoumi, H.; Degrande, G.; Lombaert, G. Prediction of free field vibrations due to pile driving using a dynamic soil–structure interaction formulation. *Soil Dyn. Earthq. Eng.* **2007**, *27*, 126–143. [CrossRef]
26. Masouleh, S.F.; Fakharian, K. Application of a continuum numerical model for pile driving analysis and comparison with a real case. *Comput. Geotech.* **2008**, *35*, 406–418. [CrossRef]
27. Liyanapathirana, D.; Ekanayake, S. Application of EPS geofoam in attenuating ground vibrations during vibratory pile driving. *Geotext. Geomembranes* **2016**, *44*, 59–69. [CrossRef]
28. Lupiezowiec, M. Fem Model of Vibration Propagation in the Soil Caused by Prefabricated Driven Piles. In Proceedings of the 14th SGEM GeoConference on Science and Technologies in Geology, Exploration and Mining, Albena, Bulgaria, 17–26 June 2014; Volume 2, pp. 363–368. [CrossRef]
29. Goh, A.T.C.; Wong, K.S.; Teh, C.I.; Wen, D. Pile Response Adjacent to Braced Excavation. *J. Geotech. Geoenviron. Eng.* **2003**, *129*, 383–386. [CrossRef]
30. Korff, M.; Mair, R.J.; Van Tol, F.A.F. Pile-Soil Interaction and Settlement Effects Induced by Deep Excavations. *J. Geotech. Geo Environ. Eng.* **2016**, *142*, 04016034. [CrossRef]
31. Ng, C.W.W.; Wei, J.; Poulos, H.; Liu, H. Effects of Multipropped Excavation on an Adjacent Floating Pile. *J. Geotech. Geoenviron. Eng.* **2017**, *143*, 04017021. [CrossRef]
32. Liyanapathirana, D.; Nishanthan, R. Influence of deep excavation induced ground movements on adjacent piles. *Tunn. Undergr. Space Technol.* **2016**, *52*, 168–181. [CrossRef]
33. Soomro, M.A.; Brohi, A.S.; Bangwar, D.K.; Bhatti, S.A. 3D Numerical Modeling of Pile Group Responses to Excavation-Induced Stress Release in Silty Clay. *Eng. Technol. Appl. Sci. Res.* **2018**, *8*, 2577–2584. [CrossRef]
34. Soomro, M.A.; Mangnejo, D.A.; Bhanbhro, R.; Memon, N.A.; Memon, M.A. 3D finite element analysis of pile responses to adjacent excavation in soft clay: Effects of different excavation depths systems relative to a floating pile. *Tunn. Undergr. Space Technol.* **2019**, *86*, 138–155. [CrossRef]

35. Wang, L.; Chen, K.; Hong, Y.; Ng, C. Effect of consolidation on responses of a single pile subjected to lateral soil movement. *Can. Geotech. J.* **2015**, *52*, 769–782. [CrossRef]
36. Basile, F. Effects of tunnelling on pile foundations. *Soils Found.* **2014**, *54*, 280–295. [CrossRef]
37. Mu, L.; Huang, M.; Finno, R.J. Tunnelling effects on lateral behavior of pile rafts in layered soil. *Tunn. Undergr. Space Technol.* **2012**, *28*, 192–201. [CrossRef]
38. *Abaqus 6.14-3 [Computer Software]*; SIMULIA: Providence, RI, USA, 2019.
39. Svinkin, M.R. Minimizing Construction Vibration Effects. *Pr. Period. Struct. Des. Constr.* **2004**, *9*, 108–115. [CrossRef]
40. Elseman, I.; Abdel, R.; Mostafa, T.M. Measurement and Evaluation of Blasting ground Vibrations and Airblasts at the Limestone Quarries of Assiut Cement Company (CEMEX). *J. Eng. Sci.* **2006**, *34*, 1293–1309.
41. Athanasopoulos, G.; Pelekis, P. Ground vibrations from sheetpile driving in urban environment: Measurements, analysis and effects on buildings and occupants. *Soil Dyn. Earthq. Eng.* **2000**, *19*, 371–387. [CrossRef]
42. Grizi, A.; Athanasopoulos-Zekkos, A.; Woods, R.D. Ground Vibration Measurements near Impact Pile Driving. *J. Geotech. Geo Environ. Eng.* **2016**, *142*, 04016035. [CrossRef]
43. Serdaroglu, M.S. Nonlinear Analysis of Pile Driving and Ground Vibrations in Saturated Cohesive Soils Using the Finite Element Method. Ph.D. Thesis, University of Iowa, Iowa City, IA, USA, 2010.
44. Schümann, B.; Grabe, J. FE-based modelling of pile driving in saturated soils. In Proceedings of the 8th International Conference on Structural Dynamics, Leuven, Belgium, 4–6 July 2011; European Association for Structural Dynamics (EASD) KUL, Technological Institute of the Royal Flemish Society of Engineers, Eds.; Katholieke Universiteit Leuven: Leuven, Belgium, 2011.
45. Zhao, G.Y.; Chen, J. Dynamic property identification of soil used in shaking table test: A comparison of several methods. In Proceedings of the 14th World Conference on Earthquake Engineering, Beijing, China, 12–17 October 2008.
46. Madheswaran, C.K.; Natarajan, K.; Sundaravadivelu, R.; Boominathan, A. Effect of Trenches on Attenuation of Ground Vibration during Pile Driving. *Springer Proc. Phys.* **2008**, *2007*, 231–238. [CrossRef]
47. Masoumi, H.; Degrande, G. Numerical modeling of free field vibrations due to pile driving using a dynamic soil-structure interaction formulation. *J. Comput. Appl. Math.* **2008**, *215*, 503–511. [CrossRef]
48. Hamidi, A.; Rooz, A.F.H.; Pourjenabi, M. Allowable Distance from Impact Pile Driving to Prevent Structural Damage Considering Limits in Different Standards. *Pr. Period. Struct. Des. Constr.* **2018**, *23*, 04017029. [CrossRef]
49. McCarron, W.O. *Deepwater Foundations and Pipeline Geomechanics*; McCarron, W.O., Ed.; J. Ross Publishing: Plantation, FL, USA, 2011.
50. Golpasand, M.R.; Do, N.A.; Dias, D.; Nikudel, M. Effect of the lateral earth pressure coefficient on settlements during mechanized tunneling. *Geomech. Eng.* **2018**. [CrossRef]
51. Wiss, J.F. Construction vibrations: State-of-the-art. *J. Geotech. Eng.* **1981**, *107*, 167–181.
52. Zhang, M.; Tao, M. A Parametric Study on Factors Affecting Ground Vibrations during Pile Driving through Finite Element Simulations. In Proceedings of the GeoRisk, Atlanta, Georgia, 26–28 June 2011; pp. 931–938.
53. Liu, G.; Jerry, S.Q. A non-reflecting boundary for analyzing wave propagation using the finite element method. *Finite Elements Anal. Des.* **2003**, *39*, 403–417. [CrossRef]
54. Deeks, A.J.; Randolph, M.F. Analytical modelling of hammer impact for pile driving. *Int. J. Numer. Anal. Methods Géoméch.* **1993**, *17*, 279–302. [CrossRef]
55. Ni, Q.; Hird, C.; Guymer, I. Physical modelling of pile penetration in clay using transparent soil and particle image velocimetry. *Géotechnique* **2010**, *60*, 121–132. [CrossRef]
56. Manandhar, S.; Yasufuku, N. Vertical bearing capacity of tapered piles in sands using cavity expansion theory. *Soils Found.* **2013**, *53*, 853–867. [CrossRef]